Journal of Orthopaedic Translation 35 (2022) 1–12

Contents lists available at ScienceDirect

Journal of Orthopaedic Translation

journal homepage: www.journals.elsevier.com/journal-of-orthopaedic-translation

Exercised accelerated the production of muscle-derived kynurenic acid in skeletal muscle and alleviated the postmenopausal osteoporosis through the Gpr35/NFκB p65 pathway

Tianshu Shi [a,c,1], Yong Shi [a,c,1], Hongliang Gao [b], Yuze Ma [a,c], Qianjin Wang [a,c], Siyu Shen [a,c], Xiaoyan Shao [a,c], Wang Gong [a,c], Xiang Chen [a,c], Jian Qin [b], Jing Wu [b], Qing Jiang [a,c,**], Bin Xue [b,*]

[a] State Key Laboratory of Pharmaceutical Biotechnology, Division of Sports Medicine and Adult Reconstructive Surgery, Department of Orthopedic Surgery, Nanjing Drum Tower Hospital, The Affiliated Hospital of Nanjing University Medical School, 321 Zhongshan Road, Nanjing, 210008, Jiangsu, PR China
[b] Core Laboratory, Sir Run Run Hospital, Nanjing Medical University, Nanjing, 211166, China
[c] Branch of National Clinical Research Center for Orthopedics, Sports Medicine and Rehabilitation, PR China

ARTICLE INFO

Keywords:
Postmenopausal osteoporosis
Muscle–bone axis
Kynurenic acid
Exercise

ABSTRACT

Background: Reduced serum estrogen levels in postmenopausal patients not only aggravate bone loss but also impact myokine secretion. Emerging evidence has revealed the importance of myokines in bone metabolism, and exercise can interfere with the secretion of myokines. However, few studies have explored the impact of exercise on myokine secretion in the postmenopausal osteoporosis (PMOP) process.

Methods: Ten-weeks-old C57B/L6 female mice were used for constructing the postmenopausal osteoporosis model. The expression levels of kynurenine aminotransferases (Kats) were detected by RT-PCR and Western Blot. The concentration of serum kynurenic acid (Kyna) was detected by HPLC-MS. Micro-CT analysis was used for determine the changes of bone mineral density and the microstructure. The primary osteoblast and osteoclast were isolated from mice to determine the effect and mechanism of Kyna on the bone formation and resorption.

Results: In our research, we found a lower serum level of muscle-derived kynurenic acid (Kyna) in PMOP model mice, accompanied by a decreased level of kynurenine aminotransferases (Kats) in the gastrocnemius muscle. Moreover, treadmill-running exercise upregulated the muscle levels of KATs and increased the serum concentration of Kyna, which was positively correlated with the alleviation of bone loss. Furthermore, we found that exogenous Kyna treatment alleviated bone mineral loss and microstructure destruction in PMOP mice by inhibiting osteoclast maturation and increasing osteoblast viability. Mechanistically, we observed that Kyna reduced the NFκB p65 phosphorylation level by activating the Gpr35 receptor, which inhibited NFATc1 expression in osteoclasts and upregulated Runx2 expression in osteoblasts.

Conclusion: Our results revealed that the muscle levels of Kats and serum level of Kyna were negatively correlated with the severity of PMOP. Exercise intervention and exogenous Kyna treatment alleviated the impairment of bone microstructure through the Gpr35 receptor, paving the way for a novel therapeutic intervention in PMOP.

The Translational potential of this article: This study provides evidences that Kyna could increase the osteoblastgenesis and inhibit the osteoclastgenesis, which could be a novel therapeutic approach for osteoporosis treatment.

* Corresponding author.
** Corresponding author. State Key Laboratory of Pharmaceutical Biotechnology, Division of Sports Medicine and Adult Reconstructive Surgery, Department of Orthopedic Surgery, Nanjing Drum Tower Hospital, The Affiliated Hospital of Nanjing University Medical School, 321 Zhongshan Road, Nanjing, 210008, Jiangsu, PR China.
E-mail addresses: qingj@nju.edu.cn (Q. Jiang), xuebin@njmu.edu.cn (B. Xue).
[1] These authors have contributed equally to this work.

https://doi.org/10.1016/j.jot.2022.03.003
Received 13 December 2021; Received in revised form 22 February 2022; Accepted 9 March 2022
Available online 4 April 2022

Author contributions

Bin Xue and Qing Jiang conceived and designed the work; Tianshu Shi and Yong Shi obtained the data; Hongliang Gao, Yuze Ma and Qianjin Wang performed the treadmill experiments; Siyu Shen, Xiaoyan Shao, Wang Gong performed *in vitro* studies; Xiang Chen, Jian Qin and Jing Wu assisted in histological analysis; Tianshu Shi wrote the manuscript; Bin Xue, Qing Jiang revised the manuscript.

1. Introduction

Postmenopausal osteoporosis (PMOP) is highly prevalent in elderly women and is characterized by a decline in bone density and the destruction of bone microstructure as estrogen levels decrease [1,2]. This significant reduction in serum estrogen levels not only changes the bone metabolism balance, but also affects the functions of other organs, including the liver, adipose tissue and muscles [3–5]. Previous studies revealed that postmenopausal women have a significantly higher risk of muscle atrophy and dysfunction than matched elderly men [5–7], which could be explained by the changes in mitochondrial function in muscle cells [8,9]. Moreover, muscles and bones could be mutually regulated [10,11]. Muscle cytokines, such as IGF-1, FGF-2, and irisin, increase bone formation, while the bone-derived cytokine osteocalcin (Ocn) also alleviates insulin resistance in muscle [12–14]. However, whether changes in muscle metabolism regulate bone loss during the PMOP process remains unknown.

Tryptophan is an essential amino acid that is primarily metabolized through the kynurenine (Kyn) pathway [15,16]. Its metabolites participate in the regulation of body inflammation, immune reactions, and neuronal excitement [15,17–20]. Previous studies reported that those metabolites, including serotonin, melatonin, and Kyn, also impact bone metabolism [21–23]. Peripheral serotonin acts as a hormone to inhibit bone formation, while brain-derived melatonin acts as the neurokinin to exert a positive effect on osteogenesis [21]. Notably, kynurenic acid (Kyna) is the product of the kynurenic pathway and is formed by the catabolism of Kyn in muscle tissues [24–26]. Emerging evidence has revealed that lower Kyna levels contribute to several diseases, including Huntington disease (HD) and chronic renal failure [27,28]. Moreover, Kyna is also involved in ROS elimination and anti-inflammatory processes [29,30], which play important roles in osteoclast maturation and osteogenesis [31]. However, it remains unclear whether muscle-derived Kyna affects bone metabolism in the PMOP process.

As a reduced level of estrogen was shown to accelerate tryptophan dysmetabolism [32,33], we proposed that muscle-derived Kyna mediates bone metabolism in the pathogenesis of PMOP. In our research, exercise rebalanced bone formation and resorption to alleviate PMOP by regulating muscle-derived Kyna. In summary, our study elucidated the influence of muscle Kyna metabolism on bone mass during the PMOP process and revealed a new mechanism by which exercise improves bone mass.

2. Materials and methods

2.1. Animals

C57BL/6 mice were obtained from the Model Animal Research Center of Nanjing University (Nanjing, China). The animals were maintained under pathogen-free conditions and a 12-h light/dark cycle with access to food and water. To induce an osteoporotic mouse model, female B6 mice were ovariectomized (OVX) or subjected to a sham-operation at 10 weeks old. They were allowed one week to relax, after which the OVX and sham mice were divided into the Kyna (Aladdin, China), running, and vehicle groups. At predetermined time points for each study, all mice were euthanized and blood samples as well as gastrocnemius muscle and bone specimens (bilateral femurs/tibias) were collected for subsequent investigation. All animal experimental protocols were reviewed and approved by the Animal Care Committee of Nanjing University in accordance with Institutional Animal Care and Use Committee guidelines (2021AE01031).

2.2. Exercise training

Eleven-week-old mice, including those of the sham and OVX groups, were subjected to treadmill running training at a speed of 10 m/min for 60 min once a day. After a total of one month of training, the mice were sacrificed, and their sera and tissues, including the gastrocnemius muscle and bone, were harvested and stored at −80 °C for further analysis.

2.3. Kynurenic acid treatment

Kynurenic acid was purchased from Aladdin. Co (Shanghai, China) and dissolved in dimethyl sulfoxide at a concentration of 2 mg/mL. Kyna (5 mg/kg body weight) was injected intraperitoneally into mice with OVX-induced osteoporosis once a day according to previous studies [29]. The control group mice were injected with an equal volume of dimethyl sulfoxide at the same volume compared to treatment group. After a total of 4 weeks of injection, the mice were sacrificed, and their sera and tissues, including, the gastrocnemius muscle and bones, were harvested and stored at −80 °C for further analysis.

2.4. Inhibitor treatment

To inhibit the activation of kynurenine aminotransferases (Kats) 1, 3, and 4, PF-04859989 hydrochloride (MedChemExpress, Shanghai, China) was used during exercise training. The Kat inhibitor was injected intraperitoneally into OVX mice at a dose of 10 mg/kg body weight from the beginning of treadmill running training twice a week according to previous studies [34]. After a total of 8 injections, the mice were sacrificed, and their sera and tissues, including the gastrocnemius muscle and bones, were harvested and stored at −80 °C for further analysis.

Moreover, to determine whether Kyna regulates bone metabolism by activating Gpr35 *in vivo*, we injected CID2745687 (CID, Aladdin, Shanghai, China) into Kyna-treated mice to inhibit Gpr35 activation. CID (1 mg/kg body weight) was injected intraperitoneally into mice in the Kyna-treated group once a day according to previous studies [35]. After a total of 4 weeks of injection, the mice were sacrificed, and tissues, including serum, the gastrocnemius muscle and bones, were harvested and stored at −80 °C for further analysis.

2.5. Measurement of serum KYNA

Aliquots of 300 μL plasma samples were obtained and calibrants were vortexed for 10 s. Plasma and calibrants were prepared using SPE with 3 cc Waters HLB cartridges (Waters, MA), after which they were placed in a vacuum elution manifold. After conditioning the cartridges with MeOH (2 mL) and 1% formic acid (2 mL), the sample was passed onto the extraction cartridge with 1% formic acid (300 μL). The loaded cartridges were then washed with 1% formic acid (2 mL), while the cartridges did not run dry at any point. The cartridges were then dried for 5–10 min with a low vacuum (±20 kPa). Elution of the absorbed analytes was performed using 1% NH_4OH in water: methanol (2 mL). The eluent was evaporated under a gentle stream of nitrogen in a heater block at 40 °C. The dried residue was reconstituted with 150 μL of 1% NH_4OH in water with methanol, vortexed for 10 s, and transferred to autosampler vials, after which 10 μL of the aliquots were injected into the LC-MS/MS system. The HPLC system consisted of an LC-20 A series HPLC with a binary gradient pump, autosampler, and vacuum degasser (Shimadzu Inc, Kyoto). Analysis was performed using a Restek C18 Aqueous column of 100 × 2.1 mm dimensions (Restek, PA). The temperature of the column was maintained at 25 °C. Detection was performed with LCMS-8040, operated in both positive and negative ESI modes. A mobile phase gradient pumped at 0.2 mL/min was used to elute the analytes from the

column. Mobile phase A consisted of ammonium formate in water (0.05%, v/v, pH adjusted to 5.5 with acetic acid) while Mobile phase B consisted of 100% acetonitrile. The elution began at 5% B, increasing linearly to 80% B at 5 min, holding at 80% until 8 min and returning to 5% B at 8.2 min and re-equilibrating to 12 min. The retention times of the IS were 8.1 min in positive mode and 6.5 min in negative mode, respectively. Kyna Standard stock solution was prepared in 50 mL MeOH/water (1:49, v/v), at a final concentration of 1 μg/mL. IS stock solution was prepared by dissolving 1 mg of ethyl-4-OH-2-quin in 50 mL MeOH/water (1:49, v/v). Both stock solutions were stored at 4 °C. Spiked plasma calibrants (n = 5) were prepared via serial dilution of the stock solution of the Kyna to the following concentrations: 100, 50, 25, 5, 0.5, and 0.1 ng/mL. Calibrations were performed using the above preparation standards. Five replicates were used to establish the linear calibration equation (y = mx + c) and were analyzed using the ratio of the analyte peak area over the IS peak area, following quantitative integration using LabSolutions Ver.5.60 software. Linearity was measured as the coefficient of determination (R^2) measured from the five calibration replicates. The collision energy voltage, Q1 Pre Bais voltage, and Q3 Pre Bais voltage were adjusted to provide the highest sensitivity. In positive ESI mode, Kyna was analyzed with multiple reaction monitoring (MRM) scan with ion pairs as the quantifier and qualifier, respectively. This LC-MS/MS method enabled the measurement of Kyna with a retention time of 6.3 min.

2.6. Microcomputed tomography (micro-CT) analysis

The left femurs of mice were skinned and fixed in 4% paraformaldehyde (PFA) for 24 h and washed with PBS before scanning. Micro-CT analysis was performed according to recently published guidelines [36] using a micro-CT scanner (SkyScan, Aarselaar, Belgium). The X-ray voltage and current were set at 80 kV and 80 μA, respectively, with a resolution of 18 μm per pixel. The region from 0.05 mm below the growth plate to 5% of the femoral length (total 100 slices were chosen, which is about 0.5 mm of the femoral length) was selected for 3-dimensional histomorphometric analysis to determine trabecular bone mineral density (Tb. BMD), trabecular bone volume per tissue volume (BV/TV), bone surface per volume (BS/BV), trabecular number (Tb.N), trabecular spacing (Tb. Sp), and trabecular thickness (Tb. Th).

2.7. Histological analysis

After overnight fixation, the right femurs were decalcified in PBS with 5% EDTA for 2 weeks. Decalcified bone specimens were embedded in paraffin after dehydration and then coronally cut into 5-μm-thick slices. Bone slices were used for tartrate-resistant acid phosphatase (TRAP) staining with a kit, according to the manufacturer's instructions (Sigma–Aldrich). For osteoblast analysis, Masson's trichrome staining (KGMST8003, Keygen, China) was used to analyze the osteoblast surface (percentage of trabecular bone surface covered by osteoblasts, OB. S/BS) per bone perimeter (Ob. N/BS). The stained slices were then photographed using an Olympus BX51 phase-contrast light microscope (Olympus, Japan).

2.8. Immunohistochemistry staining (IHC)

Bone slices were dewaxed in xylene and rehydrated in diminishing concentrations of ethanol, washed with distilled water and incubated in 3% H_2O_2 for 10 min at room temperature to eliminate endogenous peroxidase activity. Antigen retrieval was performed by heating the sections for 9 min in EDTA buffer (pH 6.0). The slices were then blocked with goat serum albumin (BOSTER, Pleasanton, USA) for 1 h at room temperature, and incubated overnight with a primary antibody specific for Ocn (Abcam, Cambridge, USA) at 4 °C. The next day, the slices were washed with PBS three times and incubated with horseradish peroxidase (HRP)-conjugated secondary antibody (Santa Cruz Biotech) for 1 h. They were then washed with PBS, stained with DAB, and terminated with water. Finally, the slices were counterstained with haematoxylin and observed as previously described.

2.9. Enzyme-linked immunosorbent assay (ELISA)

The whole blood samples were centrifuged at 1000×*g* for 15 min at room temperature within 2 h of collection to obtain the serum supernatant. They were then aspirated and transferred to new Eppendorf tubes and stored at −80 °C until they were analyzed. ELISA assay kits were used to measure the serum concentration of the biomarkers BALP (Bio-Techne, USA), P1NP (Cloud-Clone, China), CTX-1 (Cloud-Clone, China), OPG (Cloud-Clone, China), and RANKL (Bio-Techne, USA), according to the manufacturer's instructions.

2.10. Cell culture

Primary osteoblasts were isolated from the calvarias of 1-day-old mice as described in previous studies [37]. Briefly, the calvarias were sacrificed by fast decapitation, and the skin and fiber texture were cleared. After that, the calvarias were incubated in PBS containing 1% trypsin and 4 mM EDTA at 37 °C for two 10-min periods (Gibco, Grand Island, NY, USA). The obtained supernatants were discarded. Subsequently, the calvarias were digested with PBS containing 200 U/ml collagenase II for 45 min. The supernatants were centrifuged and rinsed with PBS twice. Then, the cells were cultured in αMEM supplemented with 10% fetal bovine serum (FBS). For osteoblastogenesis experiments, the growth medium was supplemented with 10 nM dexamethasone, 50 μg/mL ascorbic acid and 10 mM β-glycerophosphate.

Primary osteoclasts were isolated from the femurs and tibias of 4-week-old mice as previously reported [38]. Briefly, the bone marrow cavity was flushed with cold PBS and passed through a cell mesh. The obtained supernatants were centrifuged and rinsed with PBS twice. Then, the cells were cultured in αMEM supplemented with 10% FBS and 30 ng/ml M-CSF for proliferation (R&D Systems). For osteoclastogenesis experiments, recombinant RANKL protein was added at a concentration of 50 ng/mL (R&D Systems).

The murine monocytic cell line RAW264.7 was cultured in DMEM supplemented with 10% FBS. For osteoclastogenesis experiments, recombinant RANKL protein was added at a concentration of 50 ng/mL. The murine osteoblast cell line MC3T3-E1 was cultured in α-MEM supplemented with 10% FBS.

2.11. siRNA-mediated GPR35 silencing

To knockdown GPR35 expression, specific small interfering RNAs (siRNAs) targeting GPR35 and the negative control were purchased from Santa Cruz Biotechnology (Santa Cruz, CA, USA). MC3T3-E1 cells were transfected with GPR35 siRNA and the control using Lipofectamine 3000 (Invitrogen, Shanghai, China), according to the manufacturer's instructions.

2.12. Intracellular calcium concentration detection

Cultured MC3T3-E1 cells were treated with different concentrations of Kyna for 12 h or 24 h for further research. After discarding the medium and washing the cells with PBS, we detected the intracellular calcium concentration using a Calcium Colorimetric Assay Kit (Beyotime Biotechnology), according to the manufacturer's instructions.

2.13. RNA extraction, reverse transcription and real-time PCR

DNA-free RNA from the gastrocnemius muscle and cultured cells were isolated using Trizolreagent (Takara, Shiga, Japan) with DNase treatment, while 1 μg of total RNA was reverse transcribed into cDNA. Real-time PCR was performed on a 7500 Real-Time PCR System (Applied

Biosystems, Waltham, MA, USA) using SYBR-Green master mix (TaKaRa). The samples were subjected to 40 cycles of amplification, according to the following steps: denaturation at 95 °C for 1 min, annealing at 57 °C for 30 s, and extension at 72 °C for 30 s. The relative level of each gene was normalized to glyceraldehyde-3-phosphate dehydrogenase (GAPDH) using the $2^{-\Delta\Delta Ct}$ method, while the quantitation was independent and conducted in triplicate. The primer sequences for qRT-PCR are displayed in Table 1.

2.14. Protein preparation and western blot analysis

The gastrocnemius muscle and cells were homogenized and lysed in RIPA buffer containing protease inhibitors. Total proteins were extracted via centrifugation at 13,000 g for 15 min at 4 °C. The supernatants were then collected and mixed with sample buffer containing 2% SDS and 1% 2-mercaptoethanol, and denatured the mixtures at 99 °C for 5 min. For western blot analysis, total proteins were subjected to 10% SDS-PAGE and transferred onto PVDF membranes (Bio-Rad, Richmond, CA), which were blocked in 4% non-fat milk. Primary antibodies against KAT1 (Abcam, USA), KAT3 (Abcam, USA), KAT4 (Abcam, USA), Trap (Abcam, USA), Sema 4D (R&D systems, USA), NFATc1(CST, USA), Col 1a1 (Abclonal, China), Runx2 (Abclonal, China), β-actin (Abclonal, China), and α-tubulin (Abclonal, China) were added and incubated at 4 °C overnight. The membranes were then incubated with anti-rabbit or anti-mouse HRP-conjugated secondary antibodies at room temperature for 1 h and visualized with Licor Odyssey equipment (LI-COR Biosciences, USA).

2.15. Statistical analysis

Statistical analysis was performed using GraphPad Prism 8.0 software (GraphPad Software, La Jolla, CA, USA). All data are presented as the mean ± standard deviation (SD). A two-tailed Student's t-test was used to compare the differences between two groups, and ordinary one-way ANOVA followed by Tukey's multiple comparison test was used for multiple comparisons. P-values less than 0.05 were considered statistically significant.

3. Results

3.1. Kynurenine metabolism is involved in the alleviation of bone loss by treadmill-running in PMOP mice

To investigate the changes in kynurenine metabolism during the PMOP process, we constructed a PMOP mouse model by removing the bilateral oophorectomy (OVX). Four weeks after the operation, the BMD was determined by micro-CT analysis, which revealed a lower BMD and worse microstructure in OVX mice compared with control group mice (Fig. 1 a, b). As Kats 1, 3, 4 play important roles in the kynurenine metabolism and catalyze the conversion of KYN to KYNA in muscle, we extracted the mRNA and protein for analysis. We found decreased expression of Kats 1,3,4 in the muscles of the OVX-group compared to the control group (Fig. 1 c-d) using RT-PCR and Western blotting. Furthermore, HPLC-MS analysis showed that serum kyna levels were lower the PMOP-group than in the control group (Fig. 1 e). The data demonstrated that the disturbance of kynurenine metabolism was involved in PMOP.

To explore whether the kynurenine metabolism is involved in the alleviation of bone loss after treadmill-running intervention in PMOP-model mice, we subjected ten-week-old PMOP-model mice to a running experiment for four weeks. Micro-CT analysis showed that bone mineral loss and microstructure impairment in PMOP-model mice were alleviated after running (Fig. 1 f-g). Moreover, RT-PCR detection demonstrated that the expression of Kats (1, 3, 4) in muscle tissues was increased significantly accompanied by higher serum levels of Kyna (Fig. 1 h-i), which was positively correlated with osteogenesis in PMOP-model mice after running.

However, as exercise training can have a direct effect on bone metabolism through mechanotransduction, we used a Kat inhibitor to assess the contribution of Kyn metabolism to bone formation. After inhibitor treatment for one month, we found decreased serum levels of Kyna in the run-inhibitor group (Fig. 1 j). Moreover, we also revealed lower BMDs and worse bone microstructure in the run-inhibitor group than in the run group by micro-CT analysis (Fig. 1 k-l). Despite the low level of BMD in the run-inhibitor group, it was better than that in the OVX group, which further indicated that Kyn metabolism plays an important role in alleviating bone loss during exercise training.

3.2. KYNA treatment alleviates osteoporosis in mice with PMOP

As dysregulated of the kynurenine pathway after estrogen deficiency resulted in the decreased expression of Kats in the muscle and a lower serum concentration of Kyna, which was correlated with the decline in BMD, we hypothesized that increasing the serum concentration of Kyna would improve PMOP. Therefore, we administered Kyna to the PMOP-model mice via intraperitoneal injection (5 mg/kg, once a day) for four weeks. Micro-CT analysis demonstrated that the treatment of mice with Kyna reversed the OVX-induced loss of BMD and the impairment of bone microstructure parameters, including the BV/TV, BS/BV, Tra. Se, and Tra. th (Fig. 2 a-g). Furthermore, the Oc. S/BS ratio detected via TRAP staining was also significantly decreased (Fig. 2 h-i), while the serum level of an osteoclast biomarker, CTX-1, was decreased by 27.8% (Fig. 2 j) in the Kyna-OVX group compared to the DMSO-OVX group. Additionally, the Ob. S/BS ratio detected by IHC staining for Ocn was significantly increased (Fig. 2 l-m) in the Kyna-OVX group compared to the DMSO-OVX group, while the serum levels of the osteoblast

Table 1
Primer sequences used for quantitative PCR.

Primer	Forward (5′–3′)	Reverse (5′–3′)
KAT1	CGAAGGCTGGAAGGGATCG	GCGGTGAGAAGTCAGGGAA
KAT2	ATGAATTACTCACGGTTCCTCAC	AACATGCTCGGGTTTGGAGAT
KAT3	TTCAAAAACGCCAAACGAATCG	GATGACCAAAGCCTCTTGTGT
KAT4	GGACCTCCAGATCCCATCCT	GGTTTTCCGTTATCATCCCGGTA
Trap	CACTCCCACCCTGAGATTTGT	CATCGTCTGCACGGTTCTG
Mmp9	CTGGACAGCCAGACACTAAAG	CTCGCGGCAAGTCTTCAGAG
Ctsk	GAAGAAGACTCACCAGAAGCAG	TCCAGGTTATGGGCAGAGATT
NFATc1	GGAGCGGAGAAACTTTGCG	GTGACACTAGGGGACACATAACT
Calcineurin	TTACGGAGGTATGCGCTGAC	ATGCGGGGAGCAGTTGAAC
Collagen 1a1	GTAACTTCGTGCCTAGCAACA	CCTTTGTCAGAATACTGAGCAGC
Alpl	CCAACTCTTTTGTGCCAGAGA	GGCTACATTGGTGTTGAGCTTTT
OCN	CTGACCTCACAGATCCCAAGC	TGGTCTGATAGCTCGTCACAAG
SP7	ATGGCGTCCTCTCTGCTTG	TGAAAGGTCAGCGTATGGCTT
Runx2	ATGCTTCATTCGCCTCACAAA	GCACTCACTGACTCGGTTGG
GAPDH	AGGTCGGTGTGAACGGATTTG	TGTAGACCATGTAGTTGAGGTCA

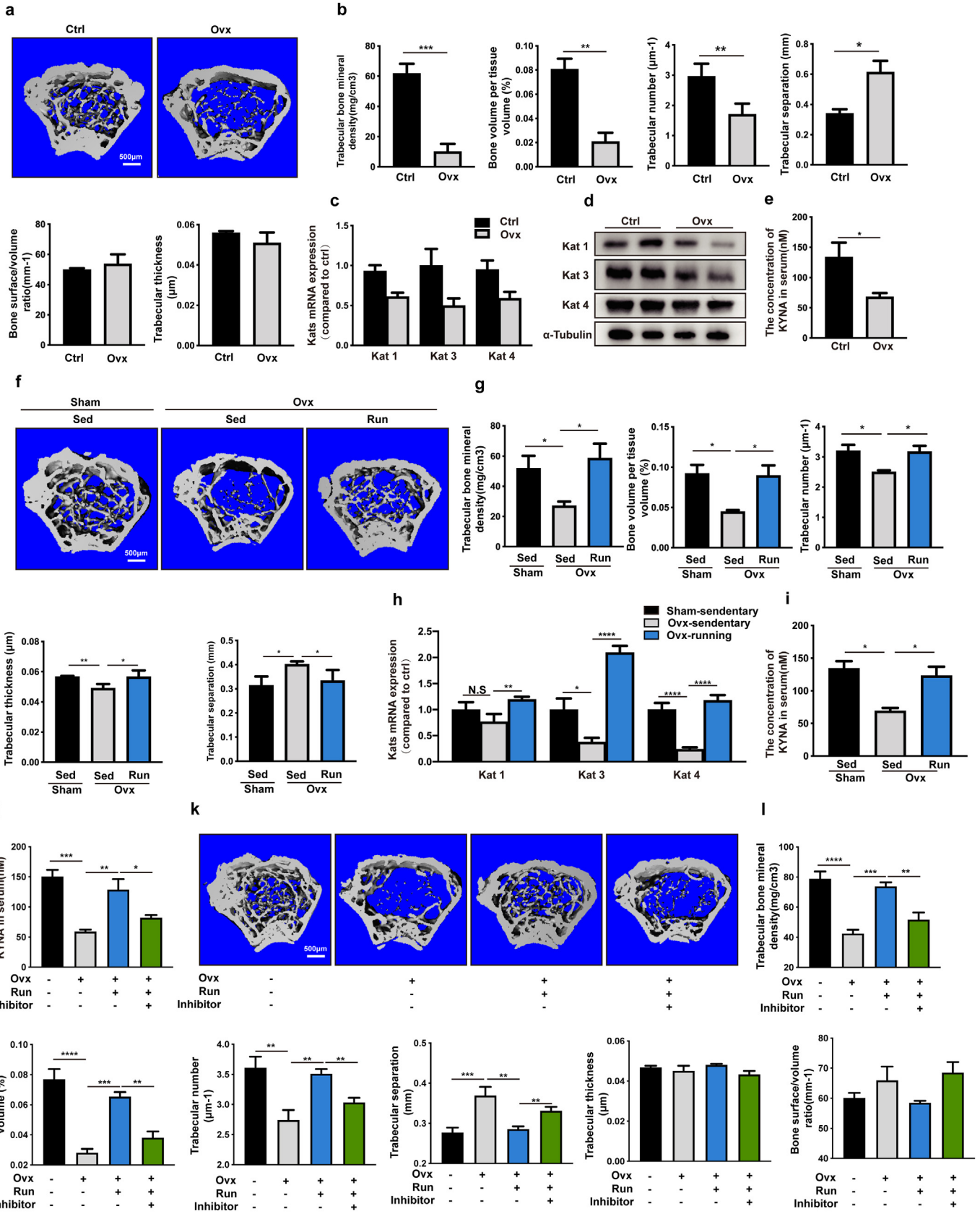

(caption on next page)

Fig. 1. Kynurenine metabolism involved in treadmill-running induced the alleviation of bone loss in PMOP-model mice. **a.** Representative micro-CT images of femoral trabecular bones from OVX- or sham-operated mice. **b.** Histomorphometric analysis of femurs from mice in each group (n = 4), including Trabecular bone mineral density (BMD), bone volume per tissue volume (BV/TV), bone surface/volume ratio (BS/BV), trabecular number (Tb.N), trabecular thickness (Tb.Th) and trabecular separation (Tb.Sp). **c.** Quantitative real-time PCR (qRT-PCR) analysis of mRNA expression of Kats in skeletal muscles from OVX- or sham-operated mice (n = 3). **d.** Western blot analysis of Kat 1, 3 and 4 protein expression in skeletal muscles from Ovx- or Ctrl mice (n = 2). **e.** Serum concentration of kynurenic acid (Kyna) (n = 4–6). **f.** Representative micro-CT images of femoral trabecular bones from Ovx- or sham-operated mice with or without running. **g.** Histomorphometric analysis of femurs from mice in each group (n = 3–5), including BMD, BV/TV, BS/BV, Tb.N, Tb.Th and Tb. Sp. **h.** The mRNA expression of Kat1, 3, 4 in gastrocnemius muscle of OVX-induced mice with or without running; **i.** Serum level of Kyna in OVX-induced mice with or without running. **j.** Serum level of Kyna in different groups (n = 3–5). **k.** Representative micro-CT images of femoral trabecular bones. **l.** Histomorphometric analysis of femurs from mice in each group (n = 3–5), including BMD, BV/TV, BS/BV, Tb.N, Tb.Th and Tb. Sp. Results are shown as mean ± SEM. $^{*}P < 0.05$, $^{**}P < 0.01$, $^{***}P < 0.001$ and $^{****}P < 0.0001$; N.S not statistically significant by two-tailed Student's t-test (**b, c**) or ordinary one-way ANOVA with Tukey's multiple comparison test (**g, h, j, l**).

biomarkers, BALP and P1NP, were higher (Fig. 2 n, SupFig. 1 a) in the Kyna-OVX group than in the DMSO-OVX group. Additionally, we extracted the mRNA from bone tissues and found lower levels of osteoclast-related genes (Fig. 2 k) and higher levels of osteoblast-related genes (Fig. 2 o) in the Kyna-OVX group than in the DMSO-OVX group. Overall, the above data showed that Kyna supplementation can alleviate bone loss and bone microstructure impairment by rebalancing the bone formation and resorption in PMOP mice.

3.3. KYNA inhibits osteoclast maturation through GPR35 signaling

Our *in vivo* studies demonstrated that Kyna treatment decrease bone resorption by inhibiting osteoclast maturation. As such, we treated primary osteoclasts with Kyna at different concentrations for 24 h. The CCK8 results demonstrated that the viability of primary osteoclasts was not affected by Kyna (Fig. 3 a). Trap staining revealed fewer Trap-positive cells in the 50 μM and 100 μM Kyna treatment groups (Fig. 3 b-c). RT-PCR and Western blot analysis also showed lower levels of osteoclast biomarkers (*Ctsk*, *Mmp9*, and *Trap* at the mRNA levels and Trap, Sema4D at the protein level) (Fig. 3 d-e). Notably, the administration of Kyna significantly decreased the mRNA and protein levels of NFATc1, an important transcription factor in osteoclast differentiation (Fig. 3 f). The above data suggest that Kyna inhibits the maturation of primary osteoclasts.

Previous studies have demonstrated that Kyna activates G-protein-coupled receptor 35 (Gpr35) in adipocytes to regulate the energy metabolism [29]. Therefore, we assessed whether Kyna augments osteoclast differentiation by activating Gpr35. We then transfected siGpr35 into the RAW264.7 osteoclast cell line. After 24 h of transfection, the mRNA levels of osteoclast maturation biomarkers (*Nfatc1, Trap, Mmp9,* and *Ctsk*) were significantly higher in the Kyna + siRNA group than in the Kyna-only treatment group (Fig. 3 g). Furthermore, we used the CID2745687 (CID), a specific inhibitor of Gpr35, to block Gpr35 function in primary osteoclasts, As expected, the CID-induced blocking of Gpr35 increased the numbers of Trap-positive cells and decreased the mRNA levels of *Nfatc1*, *Trap*, and *Ctsk* mRNA (Fig. 3 h-i) compared to those in the control group.

To further determine whether Kyna inhibits bone resorption by activating Gpr35 *in vivo*, we injected CID2745687 (CID), a specific inhibitor of Gpr35, into Kyna-treated mice. After 4 weeks of injection, we observed lower BMDs and worse bone microstructure in the Kyna-inhibitor group than in the Kyna group (SupFig. 2a and b). Trap staining also demonstrated a higher ratio of Oc. S/BS after inhibitor treatment (Fig. 3 j-k) in the Kyna-inhibitor group, which further demonstrated that Kyna activated Gpr35 to inhibit bone resorption.

3.4. KYNA increased the osteoblast viability through GPR35 signaling

To investigate the mechanism of Kyna in bone formation, we isolated primary osteoblasts for further research. CCK8 assays showed increased cell viability after different with different concentrations of Kyna (Fig. 4 a). Moreover, osteogenesis and osteoblast mineralization were accelerated by 20 μM and 50 μM Kyna treatment as determined by ALP staining and Alizarin Red staining (Fig. 4 b,c), which was confirmed by the detection of increased mRNA and protein of osteogenesis-related genes (*Runx2*, *Col1α1*, *Alpl*, and *Ocn*) after Kyna treatment (Fig. 4 d-h).

To further determine whether Kyna increased osteogenesis by activating Gpr35, we used an siRNA to knockdown Gpr35. RT-qPCR analysis showed that the Kyna-siGpr35 group showed significantly lower mRNA expression levels of osteoblast differentiation markers, including *Runx2*, *Col1α1*, *Alpl*, and *Ocn*, than the Kyna group (Fig. 4 i-k). These results were consistent with those achieved with the Gpr35 inhibitor CID (Fig. 4 m-p). Moreover, after both Kyna and CID treatment, we observed decreased levels of osteogenesis and mineralization via ALP staining and Alizarin Red staining compared to those in the Kyna group (Fig. 4 l). Furthermore, CID treatment significantly decreased the ratios of the osteoblast surface per bone surface (Ob. S/BS) in the Kyna-inhibitor group compared to the Kyna group *in vivo* (Fig. 4 q). In summary, Kyna treatment increases Runx2 expression and accelerate the osteogenesis and mineralization of primary osteoblasts by activating Gpr35.

3.5. KYNA rebalances bone metabolism via the Gpr35/p–NF–κB P65 pathway

Previous research has demonstrated that NF-κB P65 exerts a bidirectional effect on bone formation and resorption [39]. As such, we hypothesized that NF-κB signalling mediates Kyna-induced osteogenesis. First, we observed higher levels of NF-κB P65 phosphorylation in osteoblasts and osteoclasts of PMOP-model mice. As expected, treatment with Kyna obviously inhibited the phosphorylation of NF-κB P65 (Fig. 5 a, SupFig. 3 a). In accordance with the *in vivo* assay results, Kyna also reduced NF-κB P65 phosphorylation in primary osteoblasts and osteoclasts (Fig. 5 b) (see Fig. 6).

Furthermore, we treated both primary osteoblasts and osteoclasts with TNF-α, an agonist of NF-κB P65 for 6-h. TNF-α rescued the decrease in the phosphorylation of NF-κB P65 induced by KYNA (Fig. 5 c, f). The osteogenesis and mineralization of primary osteoblasts were significantly inhibited in the TNF-α+Kyna group (Fig. 5 d-e, SupFig. 3 b). Moreover, in primary osteoclasts, we observed higher levels of NF-κB P65 phosphorylation (Fig. 5 f) and NFATc1 expression as well as accelerated osteoclast differentiation in the TNF-α+ Kyna group compared to the Kyna group (Fig. 5 g-h, SupFig. 3 c).

To determine whether Gpr35 mediated the impact of Kyna on NF-κB P65 phosphorylation, we used CID to inhibit the Gpr35 function. Higher levels of NF-κB P65 phosphorylation were observed in both primary osteoblasts and osteoclasts of the CID + Kyna group compared to the Kyna group (Fig. 5 i), which was consistent with the results of IHC staining for NF-κB P65 phosphorylation (Fig. 5 j). These results indicated that Kyna activates Gpr35 to decrease NF-κB phosphorylation and thereby inhibit osteoclast maturation and osteoblast differentiation.

4. Discussion

Postmenopausal osteoporosis (PMOP) is highly prevalent in elderly women and is characterized by decreased bone density and the destruction of bone microstructure as estrogen levels decrease [1,2]. In our study, we observed decreased expression levels of muscle KATs in PMOP-model mice, accompanied by a decreased serum concentration of

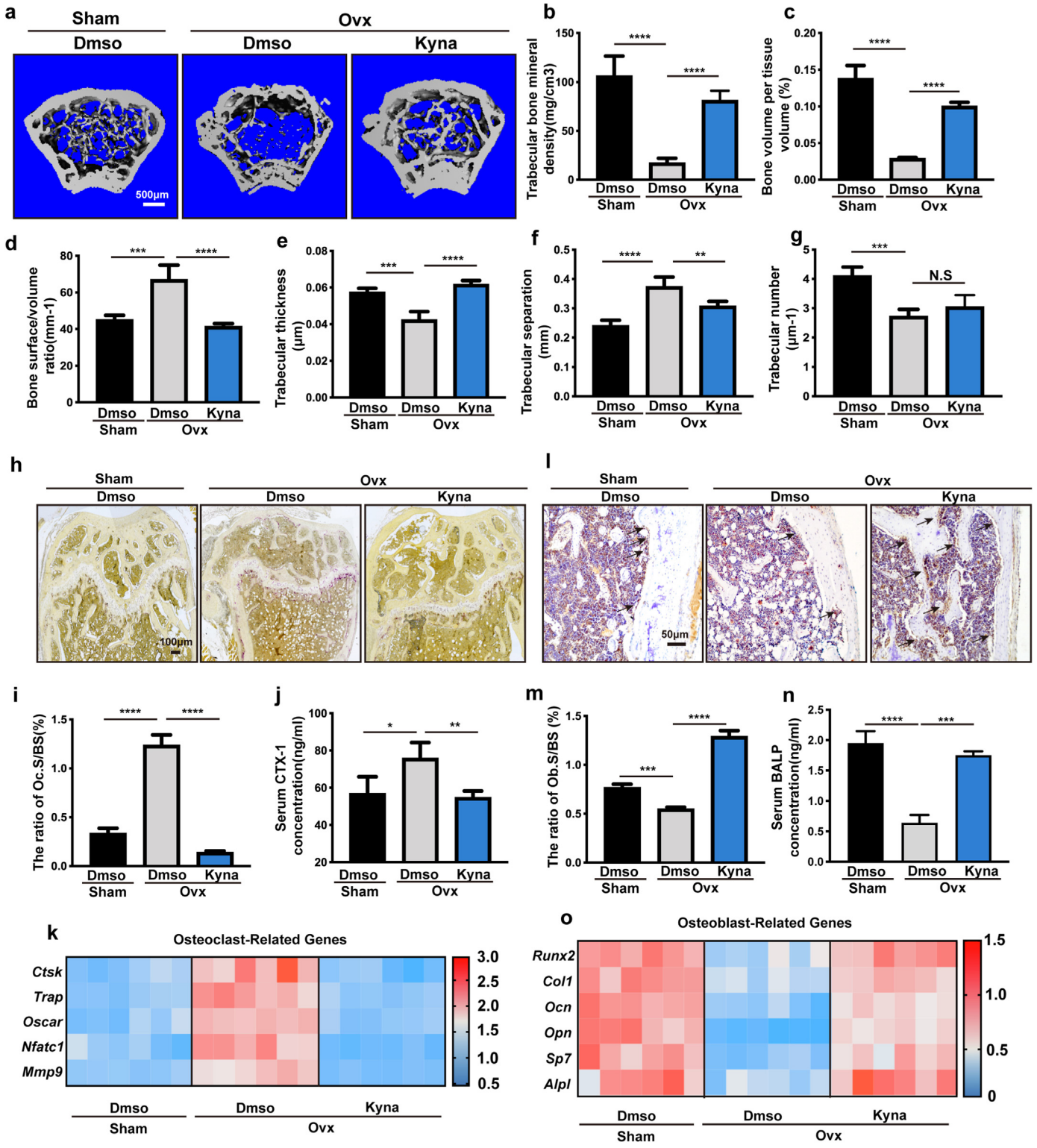

Fig. 2. KYNA treatment alleviates bone loss after OVX through dual function on bone formation and bone resorption. **a.** Representative micro-CT images of femoral trabecular bones. **b-g.** Histomorphometric analysis of femurs from mice in each group (n = 3–5). **B** Trabecular bone mineral density (BMD), **c** bone volume per tissue volume (BV/TV), **d** bone surface/volume ratio (BS/BV), **e** trabecular number (Tb.N), **f** trabecular thickness (Tb.Th), **g** trabecular separation (Tb.Sp). **h.** TRAP staining of femur sections from mice in each group (n = 3–5). **i.** Positive area quantification of TRAP staining by osteoclast surface per bone surface (Oc.S/BS). **j.** Serum concentration of CTX-1 (n = 3–5). **k.** The mRNA expression of osteoclast-related genes, including *Ctsk, Trap, Oscar, Nfatc1, Mmp9*. **l.** Immunohistochemical staining for osteocalcin (Ocn) of femur sections from mice in each group (n = 3–5). **m.** Positive area quantification by osteoblast surface per bone surface (Ob.S/BS). **n.** Serum concentration of BALP (n = 3–5). **o.** The mRNA expression of osteoblast-related genes, including *Runx2, Col1, Ocn, Opn, Sp7, Alpl*. Results are shown as mean ± SEM. $^{*}P < 0.05$, $^{**}P < 0.01$, $^{***}P < 0.001$ and $^{****}P < 0.0001$; N.S not statistically significant by ordinary one-way ANOVA with Tukey's multiple comparison test (**b-g, i, j, m, n**).

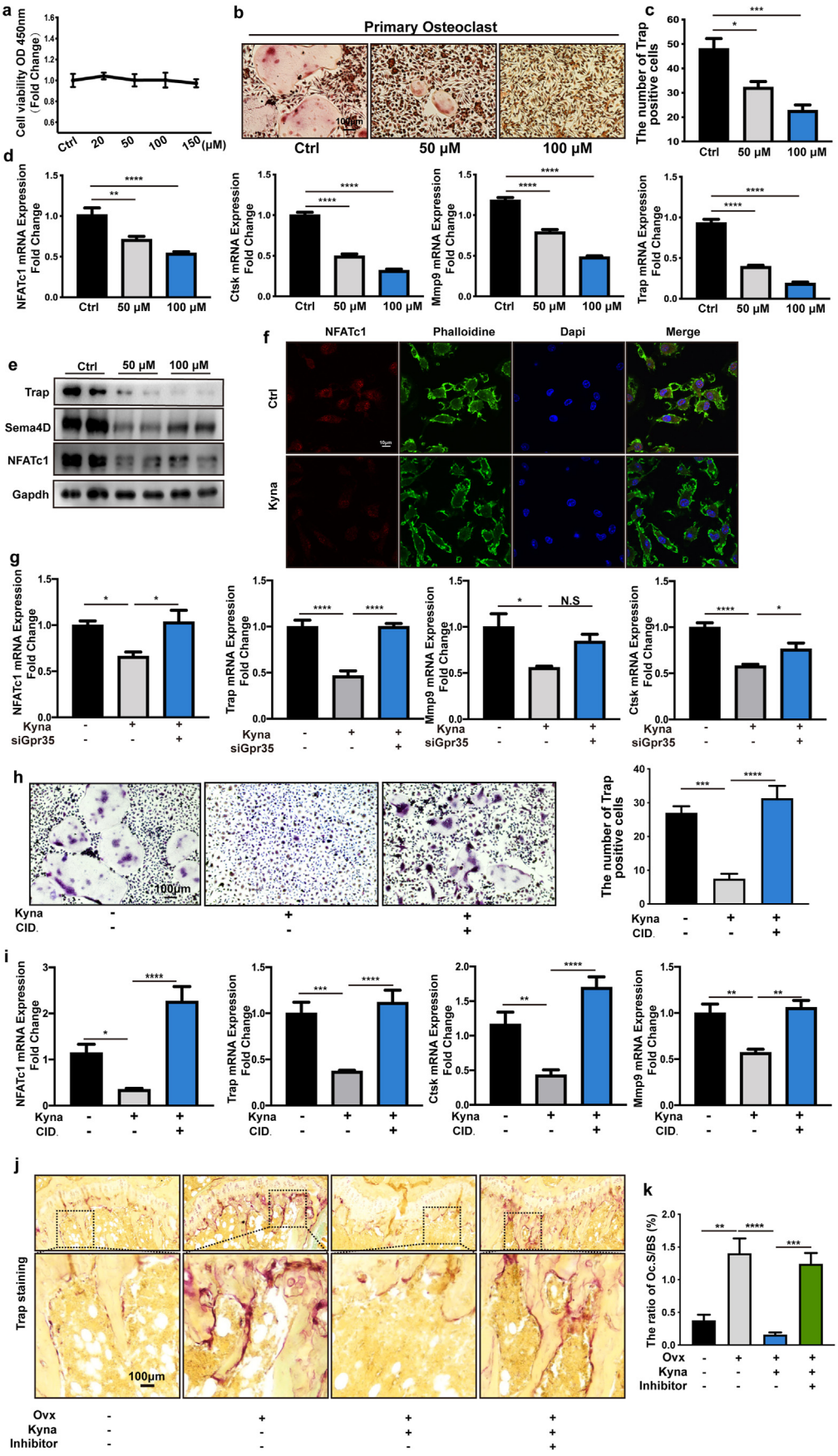

Fig. 3. KYNA inhibited the osteoclast differentiation through activating the Gpr35 reporter. **a.** The cell viability of primary osteoclast after treating with different concentrations of Kyna. **b-c.** The Trap staining (**b**) and the Trap-positive cells counting of primary osteoclast (**c**) after 50 μM and 100 μM Kyna treatment. **d.** The mRNA expression of *NFATc1, Ctsk, Mmp9* and *Trap* in primary osteoclast after 50 μM and 100 μM Kyna treatment. **e.** The protein level of Trap, Sema4D, NFATc1 in primary osteoclast after 50 μM and 100 μM Kyna treatment. **f.** The immunofluorescent of NFATc1 in primary osteoclast after 50 μM Kyna treatment. **g.** The mRNA expression of *NFATc1, Ctsk, Mmp9* and *Trap* in primary osteoclast after 50 μM Kyna treatment with or without siGpr35 treatment. **h.** The representative images of Trap staining (**Left**) and the number of trap-positive cells (**Right**) in primary osteoclast after 50 μM Kyna treatment with or without CID-2745687 treatment. **i.** The mRNA expression of *Nfatc1, Ctsk, Mmp9 and Trap* in primary osteoclast after 50 μM Kyna treatment with or without CID-2745687 treatment. **j.** TRAP staining of femur sections from mice in each group (n = 3–5). **k.** Positive area quantification of TRAP staining by osteoclast surface per bone surface (Oc.S/BS). Results are shown as mean ± SEM. $^{*}P < 0.05$, $^{**}P < 0.01$, $^{***}P < 0.001$ and $^{****}P < 0.0001$; N.S not statistically significant by ordinary one-way ANOVA with Tukey's multiple comparison test (**c, d, g, h, i, k**).

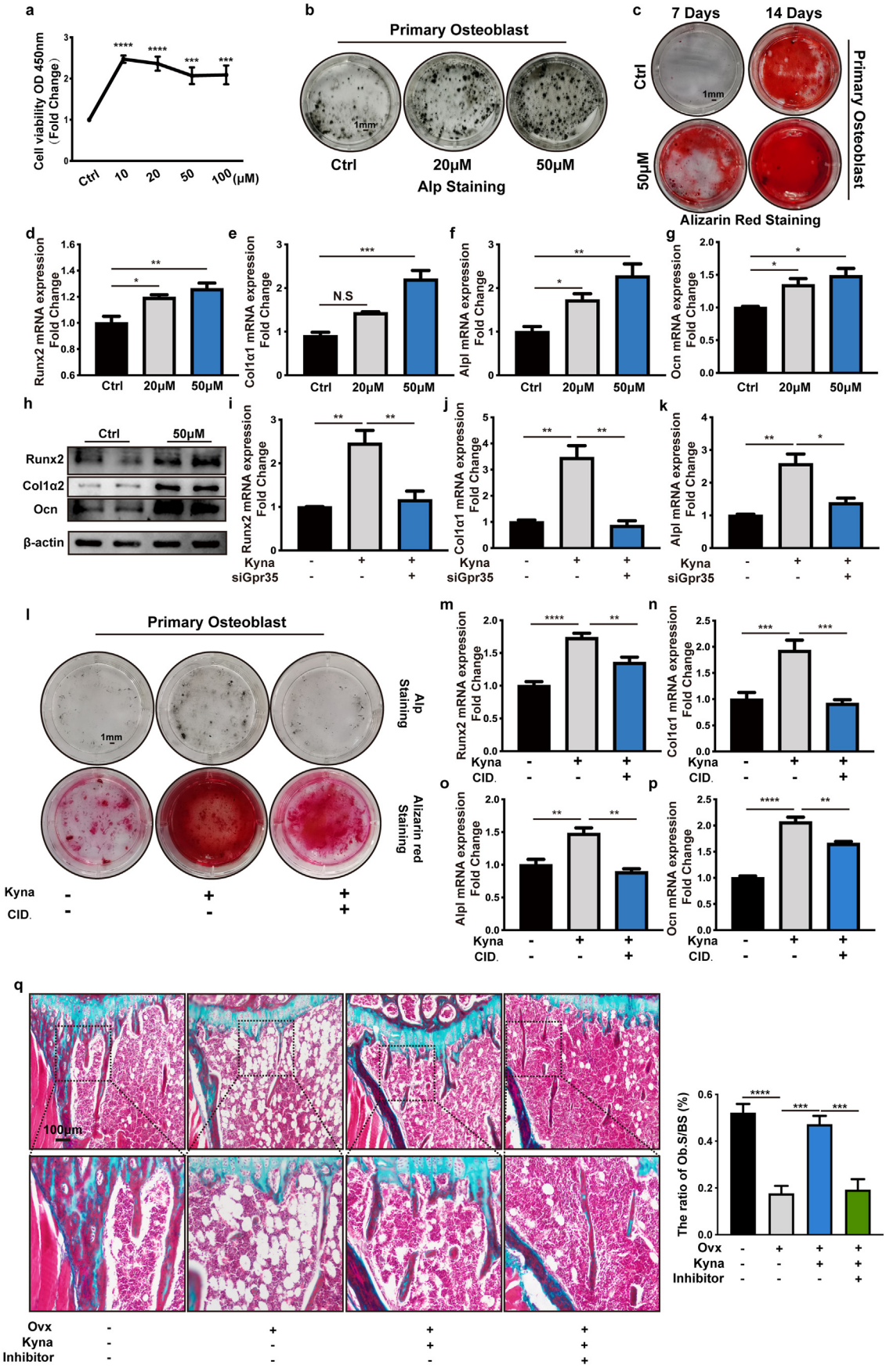

(caption on next page)

Fig. 4. KYNA promoted the osteoblast differentiation through activating the Gpr35 receptor. **a.** The cell viability of primary osteoblast after treating with different concentrations of KYNA. **b-c.** The Alp staining and Alizarin Red staining of primary osteoblast after 25 μM and 50 μM Kyna treatment. **d-g.** The mRNA expression of *Runx2, Col I, Alpl, Ocn* in primary osteoblast after 25 μM and 50 μM Kyna treatment. **h.** The protein level of Runx2, Collagen I and osteocalcin in primary osteoblast after 50 μM Kyna treatment. **i-k.** The mRNA expression of *Runx2, Col I and Alpl*, in primary osteoblast after 50 μM Kyna treatment with or without siGpr35 treatment. **l.** The Alp staining and Alizarin Red staining of primary osteoblast after 50 μM KYNA treatment with or without CID-2745687 treatment. **m-p.** The mRNA expression of *Runx2, Col I and Alpl* in primary osteoblast after 50 μM Kyna treatment with or without CID-2745687 treatment. **q.** Masson staining of femur sections from mice in each group (n = 3–5) and the ratio of osteoblast surface per bone surface (Ob.S/BS). Results are shown as mean ± SEM. $^{*}P < 0.05$, $^{**}P < 0.01$, $^{***}P < 0.001$ and $^{****}P < 0.0001$; N.S not statistically significant by ordinary one-way ANOVA with Tukey's multiple comparison test (**d-g, i-k, m-p, q**).

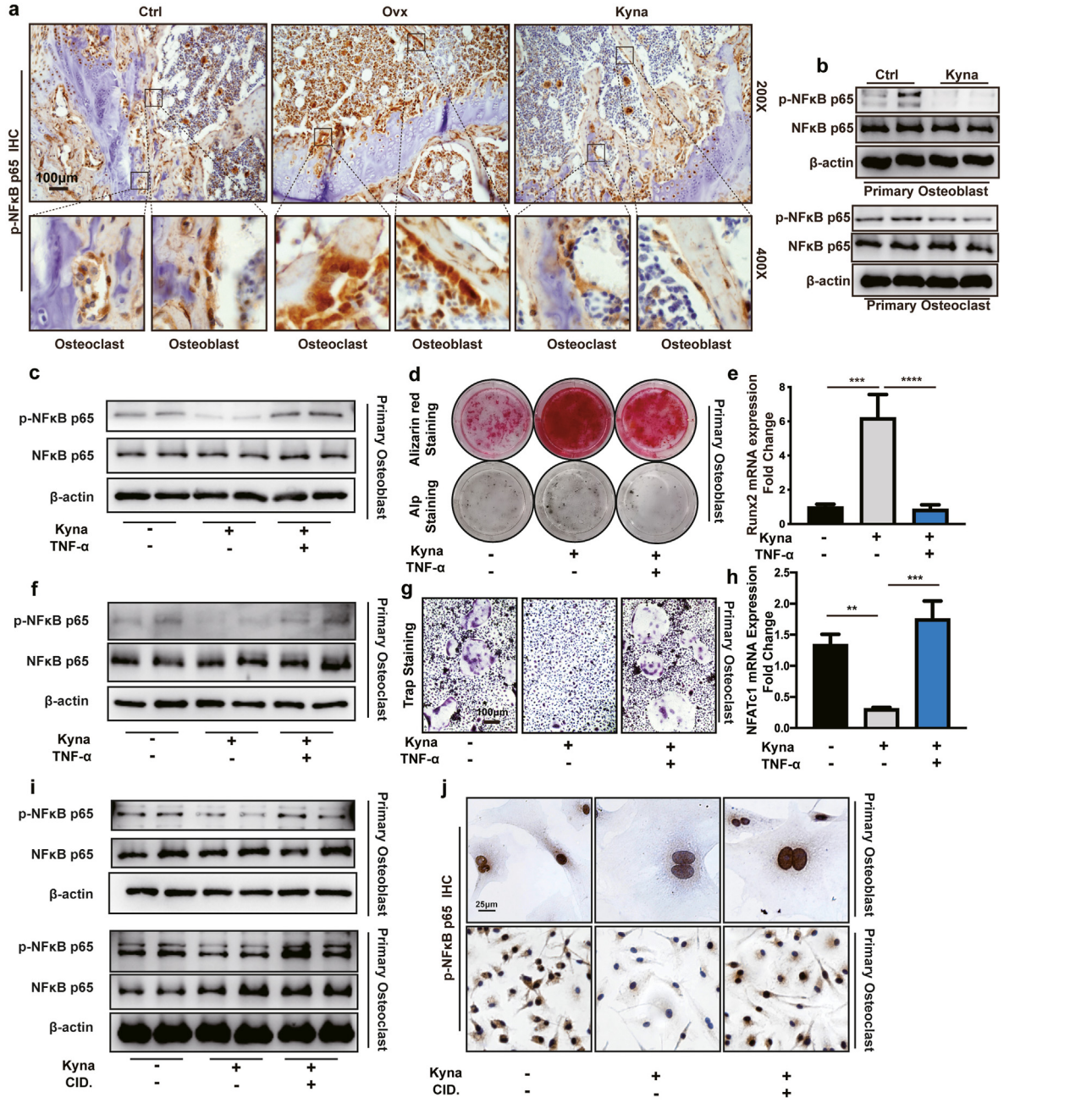

Fig. 5. KYNA induced the bone formation through inhibiting the Gpr35/p-NFκB P65 pathway. **a.** The immunohistochemical staining of p-NFκB p65 in femurs of OVX mice with or without treatment of Kyna. **b.** The protein level of p-NFκB P65 in primary osteoblast and osteoclast after 50 μM Kyna treatment. **c.** The protein level of p-NFκB P65 in primary osteoblast after 50 μM KYNA treatment with or without TNF-α treatment. **d.** The Alizarin Red staining and Alp staining of primary osteoblast after 50 μM Kyna treatment with or without TNF-α treatment. **e.** The mRNA expression of Runx2 in primary osteoblast after 50 μM Kyna treatment with or without TNF-α treatment. **f.** The protein level of p-NFκB P65 in primary osteoclast after 50 μM Kyna treatment with or without TNF-α treatment. **g.** The Trap staining of primary osteoclast after 50 μM Kyna treatment with or without TNF-α treatment. **h.** The mRNA expression of NFATc1 in primary osteoclast after 50 μM Kyna treatment with or without TNF-α treatment. **i.** The protein level of p-NFκB P65 in primary osteoblast and osteoclast after 50 μM Kyna treatment with or without CID-2745687. **j.** The immunohistochemical staining of p-NFκB p65 in primary osteoblast after 50 μM Kyna treatment with or without CID-2745687. Results are shown as mean ± SEM. $^{*}P < 0.05$, $^{**}P < 0.01$, $^{***}P < 0.001$ and $^{****}P < 0.0001$; N.S not statistically significant by ordinary one-way ANOVA with Tukey's multiple comparison test (**e, h**).

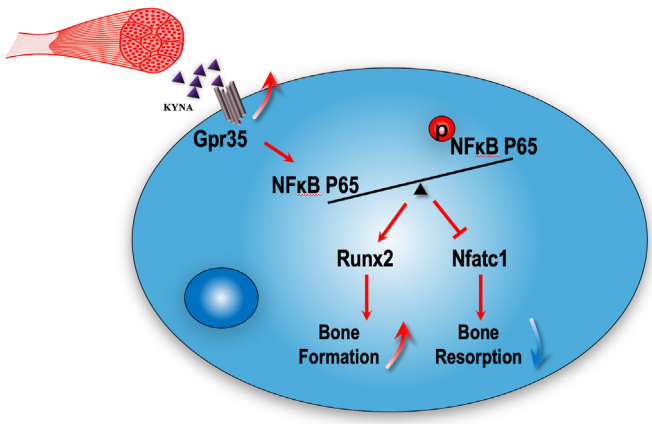

Fig. 6. Schematic diagram of the effect of Kyna on bone metabolism. Kyna: kynurenic acid; Gpr35: G protein-coupled receptor 35.

Kyna. Exercise intervention therapy and exogenous Kyna supplementation improved bone metabolism through the Gpr35/NFκB p65 pathway to inhibit bone resorption and increase bone formation in PMOP-model mice. Our research provides a novel therapeutic method for PMOP patients.

The metabolic stability of different organs is regulated by the endocrine and nervous systems [40,41]. Previous studies have found that muscles and bones are closely connected [11,14,42]. The contraction of muscles can promote bone formation by changing mechanical stimulation and accelerating the secretion of myokines [43,44]. Hyeonwoo Kim et al. reported that muscle-derived irisin could bind to the αV integrity receptor in osteocytes to decrease sclerostin expression [45]. Moreover, Camille Tagliaferri et al. summarized the myokines that positively regulate bone metabolism, including IGF-1, FGF-2, and myostatin [46]. However, in some pathological conditions, decreases in serum estrogen and androgen levels or an increase in the level of proinflammatory cytokines may increase type II muscle fiber atrophy to regulate the secretion of myogenic factors [4,47,48]. In our study, we observed low level of muscle-derived Kyna in the serum of PMOP-model mice, accompanied by decreased Kats expression in muscle. These phenomena were associated with bone loss during the pathogenesis of PMOP, thereby elucidating novel myokines affecting the bone metabolism.

Kyna is metabolized from tryptophan through kynurenine pathway [49]. Tryptophan not only participates in protein synthesis, but regulates the bodily homeostasis by being catabolized into a series of molecules through the serotonin pathway or kynurenine pathway [15,26]. Among them, the kynurenine pathway metabolizes approximately 95% of the free tryptophan via kynurenine hydroxylase and kynurenine aminotransferase, and finally produces quinolinic acid, NAD, and Kyna [16,26]. Previous studies have demonstrated that tryptophan metabolites can affect BMD [50]. Mona El Refaey et al. found that the serum accumulation of Kyn accelerated bone loss by reducing the expression of Hadc3/NCoR1 and increasing the expression of the lipid-forming gene Cidec/Plin1 in osteoclasts [23]. Kawashima, Y et al. demonstrated that quinolinic acid is required for the promotion of bone differentiation of bone marrow mesenchymal stem cells [51]. However, no studies have investigated the role of kynurenic acid in bone metabolism. Our results, herein demonstrated that treatment with Kyna for four-weeks accelerated osteoblast formation and inhibited osteoclast resorption, which alleviated bone loss. These beneficial effect of exogenous Kyna on bone further proved the advantageous effect of Kyna on bodily homeostasis, as demonstrated in previous studies on other organs, including the heart, adipocyte, and brain. This research provides a potential novel therapeutic strategy for osteoporosis treatment.

Kyna at a certain concentration can activate Gpr35, a member of the G-protein-coupled receptor family [49]. Kyna is an agonist of the aryl hydrocarbon receptor and a ligand for various receptors, including NMDA receptors, neuronal cholinergic a7 nicotine receptors, and the orphan G-coupled receptor GPR35 [52]. Importantly, we herein found the use of siGpr35 and CID2745687, an inhibitor of Gpr35, blocked the effect of Kyna on bone formation, which revealed that Gpr35 mediated the effect of Kyna on osteoblasts and osteoclasts. Moreover, Gpr35 activation was previously shown to upregulate the β-catenin levels and affect intracellular Ca^{2+} concentration, which regulates the differentiation of bone marrow stem cells through the canonical or noncanonical Wnt pathway [53–55]. Our research revealed that the activation of Gpr35 by Kyna decreased the phosphorylation of NFκB P65 in both osteoblasts and osteoclasts, which was consistent with the results of Berna Kaya et al. showing that Gpr35 deficiency increased the phosphorylation of NFκB P65 in macrophages [56].

Previous studies have demonstrated that exercise intervention therapy maintains bone mass in PMOP patients, which is caused by the increased stimulation of mechanical stress and the reduced secretion of mechanical-related factors such as sclerostin and DKK1 in osteocytes [9,57]. Additionally, the functional and metabolic changes in other organs occurring during exercise are also involved in bone formation. Exercised skeletal muscles can promote the secretion of myokines, such as irisin and IGF-1, which not only improve liver glucose metabolism but also have beneficial effects on the bone metabolism [58,59]. In our study, therapeutic intervention of PMOP with exercise increased the serum Kyna concentration by increasing the expression of the Kat enzymes in skeletal muscle, indicating that exercise intervention is an efficient therapy for PMOP.

In summary, our study revealed the dysregulated metabolism of kynurenine pathway in PMOP model mice, which significantly affected the secretion of myogenic Kyna. Exogenous Kyna supplementation significantly alleviated bone loss and bone microstructure destruction in PMOP model mice via the Gpr35/p-NFκB p65 pathway. Our findings contribute to a better understanding of the mutual regulation between muscle and skeleton under pathological conditions and provide new targets for subsequent clinical research on anti-osteoporosis drugs.

Funding/support statement

The research was supported by the National Natural Science Foundation of China (NSFC) (32071145, 31771572), Natural Science Foundation of Jiangsu Province (BK20191356), Six talent peaks project in Jiangsu Province (yy-014), Qin Lan Project of Jiangsu Province (KY520R202025), the Key R&D Program of Jiangsu Province (BE2017708), Key Program of NSFC (81730067, 82030067), Major Project of NSFC (81991514), Jiangsu Provincial Key Medical Center Foundation, Jiangsu Provincial Medical Outstanding Talent Foundation, Jiangsu Provincial Medical Youth Talent Foundation and Jiangsu Provincial Key Medical Talent Foundation. The Fundamental Research Funds for the Central Universities (14380493, 14380494), Project of Jiangsu Provincial Health Science and Technology Commission (LGY2019093).

Declaration of competing interest

The authors declare no competing interests.

Acknowledgements

All persons who have made substantial contributions to the work reported in the manuscript (e.g., technical help, writing and editing assistance, general support), but who do not meet the criteria for authorship, are named in the Acknowledgements and have given us their written permission to be named. If we have not included an Acknowledgements, then that indicates that we have not received substantial contributions from non-authors.

Appendix A. Supplementary data

Supplementary data to this article can be found online at https://doi.org/10.1016/j.jot.2022.03.003.

References

[1] Eastell R, O'Neill TW, Hofbauer LC, Langdahl B, Reid IR, Gold DT, et al. Postmenopausal osteoporosis. Nat Rev Dis Prim 2016;2:16069.
[2] Akkawi I, Zmerly H. Osteoporosis: current concepts. Joints 2018;6:122–7.
[3] Enns DL, Tiidus PM. The influence of estrogen on skeletal muscle: sex matters. Sports Med 2010;40:41–58.
[4] Ikeda K, Horie-Inoue K, Inoue S. Functions of estrogen and estrogen receptor signaling on skeletal muscle. J Steroid Biochem Mol Biol 2019;191:105375.
[5] Collins BC, Laakkonen EK, Lowe DA. Aging of the musculoskeletal system: how the loss of estrogen impacts muscle strength. Bone 2019;123:137–44.
[6] Rolland YM, Perry 3rd HM, Patrick P, Banks WA, Morley JE. Loss of appendicular muscle mass and loss of muscle strength in young postmenopausal women. J Gerontol A Biol Sci Med Sci 2007;62:330–5.
[7] Wang J, Leung KS, Chow SK, Cheung WH. Inflammation and age-associated skeletal muscle deterioration (sarcopaenia). J Orthop Translat 2017;10:94–101.
[8] Nyberg M, Egelund J, Mandrup CM, Andersen CB, Hansen Kmbe, Hergel IF, et al. Leg vascular and skeletal muscle mitochondrial adaptations to aerobic high-intensity exercise training are enhanced in the early postmenopausal phase. J Physiol 2017;595:2969–83.
[9] Gueugneau M, Coudy-Gandilhon C, Gourbeyre O, Chambon C, Combaret L, Polge C, et al. Proteomics of muscle chronological ageing in post-menopausal women. BMC Genom 2014;15:1165.
[10] Bonewald L. Use it or lose it to age: a review of bone and muscle communication. Bone 2019;120:212–8.
[11] Reginster JY, Beaudart C, Buckinx F, Bruyere O. Osteoporosis and sarcopenia: two diseases or one? Curr Opin Clin Nutr Metab Care 2016;19:31–6.
[12] Brotto M, Bonewald L. Bone and muscle: interactions beyond mechanical. Bone 2015;80:109–14.
[13] Hamrick MW. The skeletal muscle secretome: an emerging player in muscle-bone crosstalk. BoneKEy Rep 2012;1:60.
[14] Maurel DB, Jahn K, Lara-Castillo N. Muscle-bone crosstalk: emerging opportunities for novel therapeutic approaches to treat musculoskeletal pathologies. Biomedicines 2017;5.
[15] Ruddick JP, Evans AK, Nutt DJ, Lightman SL, Rook GA, Lowry CA, et al. Tryptophan metabolism in the central nervous system: medical implications. Expet Rev Mol Med 2006;8:1–27.
[16] Badawy AA. Kynurenine pathway of tryptophan metabolism: regulatory and functional aspects. 1178646917691938 Int J Tryptophan Res 2017;10.
[17] Nikolaus S, Schulte B, Al-Massad N, Thieme F, Schulte DM, Bethge J, et al. Increased tryptophan metabolism is associated with activity of inflammatory bowel diseases. e1502 Gastroenterology 2017;153:1504–16.
[18] Harden JL, Lewis SM, Lish SR, Suarez-Farinas M, Gareau D, Lentini T, et al. The tryptophan metabolism enzyme L-kynureninase is a novel inflammatory factor in psoriasis and other inflammatory diseases. J Allergy Clin Immunol 2016;137:1830–40.
[19] Schrocksnadel K, Wirleitner B, Winkler C, Fuchs D. Monitoring tryptophan metabolism in chronic immune activation. Clin Chim Acta 2006;364:82–90.
[20] Moffett JR, Namboodiri MA. Tryptophan and the immune response. Immunol Cell Biol 2003;81:247–65.
[21] Ducy P, Karsenty G. The two faces of serotonin in bone biology. J Cell Biol 2010;191:7–13.
[22] Cardinali DP, Ladizesky MG, Boggio V, Cutrera RA, Mautalen C. Melatonin effects on bone: experimental facts and clinical perspectives. J Pineal Res 2003;34:81–7.
[23] Refaey ME, McGee-Lawrence ME, Fulzele S, Kennedy EJ, Bollag WB, Elsalanty M, et al. Kynurenine, a tryptophan metabolite that accumulates with age, induces bone loss. J Bone Miner Res : Off J Am Soc Bone Miner Res 2017;32:2182–93.
[24] Stone TW. Development and therapeutic potential of kynurenic acid and kynurenine derivatives for neuroprotection. Trends Pharmacol Sci 2000;21:149–54.
[25] Liu H, Ding L, Zhang H, Mellor D, Wu H, Zhao D, et al. The metabolic factor kynurenic acid of kynurenine pathway predicts major depressive disorder. Front Psychiatr 2018;9:552.
[26] Chen Y, Guillemin GJ. Kynurenine pathway metabolites in humans: disease and healthy States. Int J Tryptophan Res 2009;2:1–19.
[27] Beal MF, Matson WR, Swartz KJ, Gamache PH, Bird ED. Kynurenine pathway measurements in Huntington's disease striatum: evidence for reduced formation of kynurenic acid. J Neurochem 1990;55:1327–39.
[28] Pawlak K, Mysliwiec M, Pawlak D. Kynurenine pathway - a new link between endothelial dysfunction and carotid atherosclerosis in chronic kidney disease patients. Adv Med Sci 2010;55:196–203.
[29] Agudelo LZ, Ferreira DMS, Cervenka I, Bryzgalova G, Dadvar S, Jannig PR, et al. Kynurenic acid and Gpr35 regulate adipose tissue energy homeostasis and inflammation. e375 Cell Metabol 2018;27:378–92.
[30] Salimi Elizei S, Poormasjedi-Meibod MS, Wang X, Kheirandish M, Ghahary A. Kynurenic acid downregulates IL-17/1L-23 axis in vitro. Mol Cell Biochem 2017;431:55–65.
[31] Agidigbi TS, Kim C. Reactive oxygen species in osteoclast differentiation and possible pharmaceutical targets of ROS-mediated osteoclast diseases. Int J Mol Sci 2019;20.
[32] Donner N, Handa RJ. Estrogen receptor beta regulates the expression of tryptophan-hydroxylase 2 mRNA within serotonergic neurons of the rat dorsal raphe nuclei. Neuroscience 2009;163:705–18.
[33] Jayawickrama GS, Nematollahi A, Sun G, Gorrell MD, Church WB. Inhibition of human kynurenine aminotransferase isozymes by estrogen and its derivatives. Sci Rep 2017;7:17559.
[34] Dounay AB, Anderson M, Bechle BM, Campbell BM, Claffey MM, Evdokimov A, et al. Discovery of brain-penetrant, irreversible kynurenine aminotransferase II inhibitors for schizophrenia. ACS Med Chem Lett 2012;3:187–92.
[35] Kim MJ, Park SJ, Nam SY, Im DS. Lodoxamide attenuates hepatic fibrosis in mice: involvement of GPR35. Biomol Ther (Seoul) 2019:92–7.
[36] Bouxsein ML, Boyd SK, Christiansen BA, Guldberg RE, Jepsen KJ, Muller R, et al. Guidelines for assessment of bone microstructure in rodents using micro–computed tomography. J Bone Miner Res 2010;25:1468–86.
[37] Gao J, Feng Z, Wang X, Zeng M, Liu J, Han S, et al. SIRT3/SOD2 maintains osteoblast differentiation and bone formation by regulating mitochondrial stress. Cell Death Differ 2018;25:229–40.
[38] Fu L, Wu W, Sun X, Zhang P. Glucocorticoids enhanced osteoclast autophagy through the PI3K/Akt/mTOR signaling pathway. Calcif Tissue Int 2020;107:60–71.
[39] Guo W, Li H, Lou Y, Zhang Y, Wang J, Qian M, et al. Tyloxapol inhibits RANKL-stimulated osteoclastogenesis and ovariectomized-induced bone loss by restraining NF-kappaB and MAPK activation. J Orthop Translat 2021;28:148–58.
[40] Steinman L. Elaborate interactions between the immune and nervous systems. Nat Immunol 2004;5:575–81.
[41] Gibson A. The influence of endocrine hormones on the autonomic nervous system. J Auton Pharmacol 1981;1:331–58.
[42] Kang YJ, Yoo JI, Baek KW. Differential gene expression profile by RNA sequencing study of elderly osteoporotic hip fracture patients with sarcopenia. J Orthop Translat 2021;29:10–8.
[43] Zhang J, Valverde P, Zhu X, Murray D, Wu Y, Yu L, et al. Exercise-induced irisin in bone and systemic irisin administration reveal new regulatory mechanisms of bone metabolism. Bone Res 2017;5:16056.
[44] Kawao N, Kaji H. Interactions between muscle tissues and bone metabolism. J Cell Biochem 2015;116:687–95.
[45] Kim H, Wrann CD, Jedrychowski M, Vidoni S, Kitase Y, Nagano K, et al. Irisin mediates effects on bone and fat via alphaV integrin receptors. Cell 2019;178:507–8.
[46] Tagliaferri C, Wittrant Y, Davicco MJ, Walrand S, Coxam V. Muscle and bone, two interconnected tissues. Ageing Res Rev 2015;21:55–70.
[47] Tournadre A, Vial G, Capel F, Soubrier M, Boirie Y Sarcopenia. Joint Bone Spine 2019;86:309–14.
[48] Yang W, Hu P. Skeletal muscle regeneration is modulated by inflammation. J Orthop Translat 2018;13:25–32.
[49] Wang J, Simonavicius N, Wu X, Swaminath G, Reagan J, Tian H, et al. Kynurenic acid as a ligand for orphan G protein-coupled receptor GPR35. J Biol Chem 2006;281:22021–8.
[50] Al Saedi A, Sharma S, Summers MA, Nurgali K, Duque G. The multiple faces of tryptophan in bone biology. Exp Gerontol 2020;129:110778.
[51] Kawashima Y, Sanaka T, Sugino N, Takahashi M, Mizoguchi H. Suppressive effect of quinolinic acid and hippuric acid on bone marrow erythroid growth and lymphocyte blast formation in uremia. Adv Exp Med Biol 1987;223:69–72.
[52] Olenchock BA, Moslehi J, Baik AH, Davidson SM, Williams J, Gibson WJ, et al. EGLN1 inhibition and rerouting of alpha-ketoglutarate suffice for remote ischemic protection. Cell 2016;164:884–95.
[53] Zhang Y, Shi T, He Y. GPR35 regulates osteogenesis via the Wnt/GSK3beta/beta-catenin signaling pathway. Biochem Biophys Res Commun 2021;556:171–8.
[54] Berlinguer-Palmini R, Masi A, Narducci R, Cavone L, Maratea D, Cozzi A, et al. GPR35 activation reduces Ca2+ transients and contributes to the kynurenic acid-dependent reduction of synaptic activity at CA3-CA1 synapses. PLoS One 2013;8:e82180.
[55] Jung TW, Park J, Sun JL, Ahn SH, Abd El-Aty AM, Hacimuftuoglu A, et al. Administration of kynurenic acid reduces hyperlipidemia-induced inflammation and insulin resistance in skeletal muscle and adipocytes. Mol Cell Endocrinol 2020;518:110928.
[56] Kaya B, Donas C, Wuggenig P, Diaz OE, Morales RA, Melhem H, et al. Lysophosphatidic acid-mediated GPR35 signaling in CX3CR1(+) macrophages regulates intestinal homeostasis. Cell Rep 2020;32:107979.
[57] Belavy DL, Baecker N, Armbrecht G, Beller G, Buehlmeier J, Frings-Meuthen P, et al. Serum sclerostin and DKK1 in relation to exercise against bone loss in experimental bed rest. J Bone Miner Metabol 2016;34:354–65.
[58] Huh JY. The role of exercise-induced myokines in regulating metabolism. Arch Pharm Res 2018;41:14–29.
[59] Pedersen BK, Febbraio MA. Muscles, exercise and obesity: skeletal muscle as a secretory organ. Nat Rev Endocrinol 2012;8:457–65.